Dalton Transactions

PAPER

View Article Online
View Journal | View Issue

Cite this: *Dalton Trans.*, 2017, **46**, 11425

Fine tuning of catalytic and sorption properties of metal–organic frameworks *via in situ* ligand exchange†

Peng Wang,[a] Kai Chen,[a] Qing Liu,[a] Huai-Wei Wang,[a] Mohammad Azam,[b] Saud I. Al-Resayes,[b] Yi Lu*[a] and Wei-Yin Sun *[a]

Received 20th June 2017,
Accepted 2nd August 2017

DOI: 10.1039/c7dt02231j

rsc.li/dalton

Metal–organic frameworks (MOFs) are gaining considerable attention not only because of their diverse structures but also due to their interesting properties and potential applications. However, fabrication of MOFs with desired structures and properties remains a great challenge. In this study, a strategy based on ligand exchange *via* single-crystal-to-single-crystal (SCSC) transformation has been undertaken, which can be used to achieve MOFs not available by direct synthesis and also to enrich the family of isoreticular MOFs. Direct X-ray crystallographic observation provides undoubted evidence that the pyrazine (pyz) ligand in $[Cu_3(L)_2(pyz)(H_2O)]$ (L^{3-} = [1,1′:3′,1″-terphenyl]-4,4″,5′-tricarboxylate) was replaced by its derivatives without damaging the framework. Furthermore, the catalytic and sorption properties of the MOFs are able to be fine-tuned by introducing definite substituent group decorated on the pore surface. Thus, it is expected that the ligand exchange will be powerful for replacing linker molecules with others having desirable substituents, and as a result to afford desired MOFs.

Introduction

Metal–organic frameworks (MOFs), consisting of inorganic building blocks and organic bridging linkers, have attracted remarkable attention from chemists due to their interesting properties and potential applications in gas storage and separation, sensing, catalysis and so on.[1–7] A wide variety of MOFs with diverse structures have been reported in the past few decades;[8] however, it is still a significant challenge to achieve MOFs with predesigned structures and desired properties.[9] On the one hand, it is known that many factors, including organic ligand, metal center, reaction solvent, temperature *etc.*, can affect the resultant structures of MOFs,[10,11] which make it difficult to predict and control the final MOFs formed. On the other hand, in some cases it is difficult to characterize the products, for example complicated reactions without pure phase crystalline products. Thus, there are reports in recent studies on the post-synthesis modification (PSM) strategy, aiming to construct MOFs retaining their structural integrity after modification.[12,13] In addition, central metal ion exchange was used to improve the properties of MOFs.[14] Also, organic linker exchange was found to be useful in the synthesis of unattainable MOFs.[15–17] Both metal ion and organic ligand exchanges are demonstrated to be effective in the fabrication of MOFs; however, normally it is difficult to determine the completion or the extent of exchange. Further direct evidence is required.

In this study, a strategy based on ligand exchange *via* single-crystal-to-single-crystal (SCSC) transformation of MOFs has been employed.[18] The direct X-ray crystallographic observation provides undoubted evidence of complete ligand exchange in the MOFs, and more importantly this can be used to achieve MOFs not available by direct synthesis. We reported a MOF $[Cu_3(L)_2(DABCO)(H_2O)]\cdot 15H_2O\cdot 9DMF$ (**1-DABCO**) (L^{3-} = [1,1′:3′,1″-terphenyl]-4,4″,5′-tricarboxylate, DABCO = 1,4-diazabicyclo[2.2.2]octane, DMF = *N*,*N*-dimethylformide) with $[Cu_2(OCO)_4]$ paddle wheel secondary building units (SBUs) linked by DABCO.[19] The high thermal stability and large pore size of **1-DABCO** offer an ideal platform for further pore surface engineering. Considering the similar distance between the two nitrogen atoms in DABCO and pyrazine (pyz) as well as its derivatives, we started studying the replacement of DABCO in **1-DABCO** by pyz and a new MOF $[Cu_3(L)_2(pyz)(H_2O)]\cdot 13DMF$ (**1**) was achieved. Furthermore, the ligand exchange of pyz in **1** with its derivatives, namely 2,5-Me_2pyz,

[a]*Coordination Chemistry Institute, State Key Laboratory of Coordination Chemistry, School of Chemistry and Chemical Engineering, Nanjing National Laboratory of Microstructures, Collaborative Innovation Center of Advanced Microstructures, Nanjing University, Nanjing 210023, China. E-mail: sunwy@nju.edu.cn; Fax: (+) 86 25 89682309*

[b]*Department of Chemistry, College of Science, King Saud University, P. O. Box 2455, Riyadh 11451, Kingdom of Saudi Arabia*

† Electronic supplementary information (ESI) available: Syntheses and characterization of MOFs **1–6**. CCDC 1028540–1028545. For ESI and crystallographic data in CIF or other electronic format see DOI: 10.1039/c7dt02231j

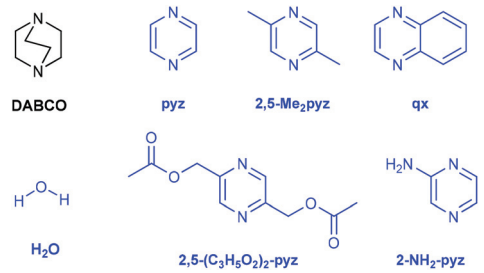

Scheme 1 Schematic illustration of the ligands used in the MOFs. DABCO = 4-diazabicyclo[2.2.2]octane, pyz = pyrazine, 2,5-Me_2pyz = 2,5-dimethylpyrazine, qx = quinoxaline, H_2O = water, 2,5-$(C_3H_5O_2)_2$-pyz = pyrazine-2,5-diylbis(methylene) diacetate and 2-NH_2-pyz = pyrazine-2-amine.

qx, 2,5-$(C_3H_5O_2)_2$-pyz and 2-NH_2-pyz as illustrated in Scheme 1 was investigated and, fortunately, complete ligand exchange with desired groups on the internal surface of the MOFs was found to proceed through the SCSC transformations, and MOFs $[Cu_3(L)_2(2,5\text{-}Me_2pyz)(H_2O)]\cdot 12DMF$ (**2**), $[Cu_3(L)_2(qx)(H_2O)]\cdot 12DMF$ (**3**), $[Cu_3(L)_2(H_2O)_2(H_2O)]\cdot 12DMF$ (**4**), $[Cu_3(L)_2(2,5\text{-}(C_3H_5O_2)_2\text{-}pyz)(H_2O)]\cdot 8DMF$ (**5**) and $[Cu_3(L)_2(2\text{-}NH_2\text{-}pyz)(H_2O)]\cdot 12DMF$ (**6**) were successfully obtained.

Experimental section

Synthesis and characterization of the compounds

The syntheses and characterization of MOFs **1–6** are described in the ESI.†

In situ X-ray diffraction

Time-dependent X-ray diffraction analysis of the ligand exchange reaction was carried out using single crystal **1** (0.5 mm × 0.5 mm × 0.4 mm) in a capillary (~0.2 ml DMF), which was injected with 10 μL qx/DMF (10^{-3} mol ml^{-1}) solution. X-ray diffraction data were collected at different times after the injection using the same single crystal.

Ligand exchange

From 1 to 3. Complex **1** (200 mg) was suspended in a DMF (10 ml) solution of qx (52 mg) at room temperature for 24 h. The solution was removed, replaced with a fresh qx/DMF (52 mg/10 ml) solution and the mixture was allowed to stand at room temperature for 24 h. The product was washed using DMF and then analyzed by ^{1}H-NMR (Fig. S10 and S12†).

From 1 to 6. Complex **1** (200 mg) was suspended in a NH_2-pyz/DMF (38 mg/10 ml) solution. The mixture was heated at 50 °C for 24 h. The solution was removed, replaced with a fresh NH_2-pyz/DMF (38 mg/10 ml) solution and the mixture was again heated at 50 °C for 24 h. The product was washed using DMF and then analyzed *via* ^{1}H-NMR (Fig. S10 and S15†).

Catalytic Knoevenagel condensation reaction

Before the reaction, the materials were soaked in cyclohexane at room temperature for 2 h to remove the DMF in the sample. In a typical experiment, 214 mg of benzaldehyde (2 mmol) and 0.1 mmol of the dried catalyst [100.7 mg of $[Cu_3(L)_2(pyz)(H_2O)]$ (**1**) or 102.2 mg of $[Cu_3(L)_2(2\text{-}NH_2\text{-}pyz)(H_2O)]$ (**6**)] were mixed in 5 ml of cyclohexane as a solvent and heated to 80 °C, and then 226 mg of ethyl cyanoacetate (2 mmol) was rapidly added into the reactor. All the catalytic reactions were carried out under N_2 in a glass flask that was equipped with a reflux condenser and a magnetic stirrer. The reactor was placed in a thermostatic oil bath. After the reaction, the catalyst was separated by filtration. The products were analyzed by ^{1}H-NMR. The conversions were calculated based on dibromomethane as an internal standard.

Results and discussion

As an isoreticular analogue of previously reported MOF $[Cu_3(L)_2(DABCO)(H_2O)]\cdot 15H_2O\cdot 9DMF$ (**1-DABCO**),[19] $[Cu_3(L)_2(pyz)(H_2O)]\cdot 13DMF$ (**1**) using pyz as a bridging linker was synthesized by the solvothermal reaction of a mixture of H_3L, $Cu(NO_3)_2\cdot 3H_2O$ and pyz in DMF at 140 °C for 72 h. The reaction gave a pure crystalline product of **1** in a high yield, that was further characterized by single crystal X-ray diffraction (Fig. 1), ^{1}H-NMR, TGA and IR (Fig. S1, S10, S17 and S23†). Furthermore, we are pleased to find that **1** can be easily prepared on the gram scale, which is important for further study and application. The results of crystallographic analysis confirm that **1** has the same structure and topology as **1-DABCO**. It is noteworthy that there are two different cages in **1** as illustrated in Fig. 1. The smaller cage A, highlighted by a violet sphere, consists of 4 $Cu_2(OCO)_4$ paddle wheel SBUs, 4 L^{3-} and 2 pyz, while the larger one (cage B), highlighted by an yellow sphere, contains 9 $Cu_2(OCO)_4$ SBUs and 8 L^{3-} and 3 pyz ligands.

To enhance the properties of MOFs by introducing functional groups as well as to enrich the family of isoreticular MOFs, reactions with pyz derivatives were investigated. However, it was found that, in contrast to the pure product

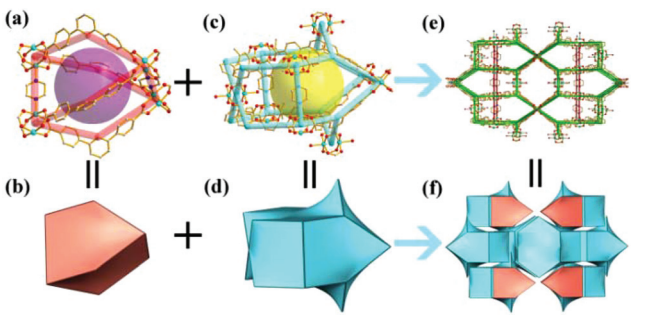

Fig. 1 Single crystal structure and topology of **1**. (a) Small cage A is highlighted with a violet sphere. (b) Simplified representation of the tiling of the small cage. (c) Large cage B is highlighted with a yellow sphere. (d) Simplified representation of the tiling of the large cage. (e) The overall structure of **1**. (f) 3D representation of the tiling of the topology.

obtained from the preparation of **1**, the reactions with pyz derivatives such as 2,5-Me_2pyz, qx (Scheme 1) instead of pyz are complex along with the formation of uncharacterizable impurities. Alternatively, we explored the ligand exchange route to access the MOFs with desired properties. As a typical example, biphasic ligand exchange experiments were performed by suspending **1** in a DMF solution of qx. ^{1}H-NMR spectral measurements confirm that the linker pyz molecule in **1** was replaced by qx at room temperature (Fig. 2a, b and Fig. S12†). It is noteworthy that the crystal of **1** remains intact and transparent upon the ligand exchange. The obtained crystals (**3**) after the exchange still have strong diffraction and are suitable for crystallographic analysis (Fig. S3†) implying an SCSC transformation of the ligand exchange process. Furthermore, the ligand exchange is reversible as evidenced by ^{1}H-NMR spectral measurements (Fig. 2b and c). The ligand exchange between **1** and **3** was performed in a DMF solution for different times at different temperatures. Interestingly, the replacement is fast even at room temperature (Fig. 2a–c) and the exchanges achieve completion as high as 98%, while in the previously reported studies, the complete ligand exchange usually requires a long reaction time ranging from a few days to several weeks.[16] And it may be attributed to different metal–ligand bonds from those of previous studies.

The SCSC transformation of ligand exchange as mentioned above encourages us to carry out *in situ* X-ray diffraction studies.[20] As shown in Fig. 2d–g and Fig. S16,† X-ray diffraction was used to capture snapshots of the reaction intermediates. The electron density change caused by the exchanged pyz derivative qx was clearly observed. The carbon atoms in pyz in **1** were disordered into two positions (Fig. 2d), while in the exchanged product **3**, no disorder was observed for qx probably due to the steric hindrance (Fig. 2g). *In situ* X-ray diffraction data provide a time dependent ligand exchange process which can be clearly seen from Fig. 2d–g and Fig. S16.† Least-square refinements converged to about 35% of pyz in **1** replaced by qx in 5 h (Fig. 2e). The exchange proceeds further with 35% of pyz and 65% of qx in the crystal in 19 h (Fig. 2f). After 31 h exchange, it is hard to find the electron residue for C atoms of pyz from the electron density map contoured at 1.0σ (Fig. 2g). The electron density map revealed that the pyz ligand in **1** gradually disappeared and was replaced by the qx ligand in **3**, preserving the stacking pattern of the structure throughout the exchange process. The structural transformations were also monitored by PXRD measurements (Fig. S7b†).

Direct observation clearly confirms the ligand exchange within the MOFs, which is beneficial for the preparation of new MOFs under mild conditions in a simple way, namely hydro-/solvothermal reactions, and purification of the reaction products can be avoided. More importantly, the ligand exchange provides a pathway for the preparation of MOFs which are not available by direct synthesis reactions. Particularly in the cases of ligands with reactive groups it may be difficult to achieve the predesigned MOFs since side reactions related to the reactive groups may occur. In the present work, we failed to get MOFs with 2,5-$(C_3H_5O_2)_2$-pyz or 2-NH_2-

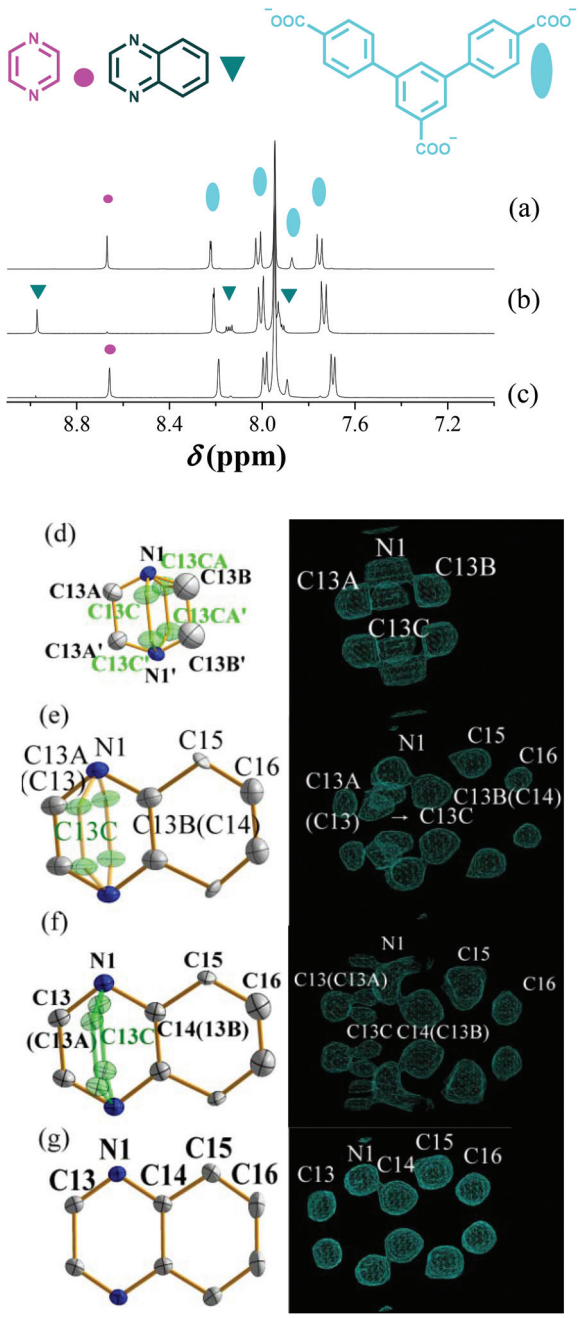

Fig. 2 NMR spectra and time-dependent X-ray diffraction data in the conversion from **1** to **3**. (a) ^{1}H-NMR spectrum of **1** after digestion; (b) ^{1}H-NMR spectrum of **1** after the exchange with 4 eq. qx three times in 5 min. (c) ^{1}H-NMR spectrum of **3** after the exchange with 4 eq. pyz three times in 5 min. (d)–(g) Time-dependent X-ray diffraction data in the conversion from **1** into **3**. Electron density maps (F_0) obtained at 15 min, 5 h, 19 h and 31 h after the addition of a DMF solution of qx. All the electron density maps are depicted within a 1.41 Å-thick slice of the pyrazine moiety and contoured at the absolute 1.0σ level.

pyz linkers through direct reactions following the same process used for the preparation of **1**, although we succeeded in the preparation of MOFs **1–4** by direct reactions (Fig. S1–S4, S7a, S10–S13, S17–S20 and S23–S26†). Under the solvothermal

reaction conditions 2,5-$(C_3H_5O_2)_2$-pyz was found to be decomposed in the presence of Cu(II) at a high temperature, while in the case of 2-NH_2-pyz, the reaction mixture becomes black (Scheme S1†) which may be due to the presence of the amino group. The results prompt us to explore the ligand exchange of **1** with 2,5-$(C_3H_5O_2)_2$-pyz and 2-NH_2-pyz linkers.

MOF **1** was suspended in a DMF solution containing excess 2-NH_2-pyz and left to undergo exchange for 0.5 h. The ^{1}H-NMR spectra reveal the presence of peaks only from 2-NH_2-pyz, implying the complete linker exchange from pyz to 2-NH_2-pyz (Fig. S15†). Single crystal X-ray diffraction analysis shows that MOF **6** obtained by ligand exchange maintains the overall framework of **1** (Fig. S6†). MOF **5** with the 2,5-$(C_3H_5O_2)_2$-pyz linker is also available from the ligand exchange from **1** with the 2,5-$(C_3H_5O_2)_2$-pyz linker (Fig. S5, S14, S21, and S27†). Above all, our results show that linkers can be systematically modified thoroughly in the whole MOFs. Such a ligand exchange method may offer a new opportunity for the construction of MOFs for specific functional groups.[21,22]

Since the stability of MOFs is important for their applications, the chemical stability of MOFs **1–6** was investigated by immersing them in $CHCl_3$, acenitrile, THF, acetone and pentane for 24 h. From the powder X-ray diffraction (PXRD) patterns, it was found that MOF **4** with water molecules instead of pyz, which has a different structure from the previously reported framework UMCM-151,[23] is unstable in most organic solvents except pentane (Fig. S8†). While the other MOFs with pyz and its derivatives show high stability to the solvents listed above, a typical example is shown in Fig. S9.† Impressively, all the samples except MOF **4** are stable in air even after weeks. Thermogravimetric analysis (TGA) of the desolvated sample of **1** showed a plateau temperature region ranging from 25 to 210 °C, indicating high thermostability (Fig. S17†). Furthermore, investigation on the PXRD patterns demonstrated that the framework of **1** retained its integrity after the removal of the guest molecules (Fig. S9†).

The porosities of **1–6** were investigated by N_2 gas adsorption at 77 K. Before sorption, the samples were exchanged by acetone except sample **4**, which was exchanged by pentane. As shown in Fig. S29,† each sample exhibits a Type I adsorption isotherm, which is characteristic of microporous materials. Interestingly, MOFs **1–6** have similar lattice parameters and their N_2 uptakes are different depending on the linkers. Significantly, **4** shows the highest N_2 uptake (867 $cm^3\ g^{-1}$). Other MOFs can take up amounts of N_2 ranging from 658 ml g^{-1} (for **5**) to 854 ml g^{-1} (for **1**). Based on these sorption data, the calculated Brunauer–Emmett–Teller (BET) surface areas ($P/P_0 < 0.15$) range from 2399 to 3207 $m^2\ g^{-1}$ and the Langmuir surface areas range from 2739 to 3727 $m^2\ g^{-1}$. By comparing **1–6** and **1-DABCO**, it is found that the surface area varies in the sequence of **4** (H_2O) > **1** (pyz) > **2** (2,5-Me_2pyz) > **3** (qx) > **1-DABCO** > **6** (2-NH_2-pyz) > **5** (2,5-$(C_3H_5O_2)_2$-pyz). MOF **5** with a large 2,5-$(C_3H_5O_2)_2$-pyz group has the smallest surface area because of the bulky linker which would diminish the accessible surface area. Moreover, MOF **4** with the smallest water molecule shows the highest surface area.[24] The high surface areas and stabilities of isoreticular **1–6** prompted us to study their CO_2 adsorption at 273 and 298 K, and the results are shown in Fig. S30–S41.† The adsorption enthalpies were calculated by fitting virial-type equations (see Table S3†). The CO_2 adsorption enthalpy at 1 bar varies in the order of **6** (2-NH_2-pyz) > **2** (2,5-Me_2pyz) > **1** (pyz) ≈ **5** (2,5-$(C_3H_5O_2)_2$-pyz) > **3** (qx) > **4** (H_2O) > **1-DABCO**, which is different from the sequence of the surface area. Particularly, it is noticeable that **6** with a 2-NH_2-pyz linker shows the largest adsorption enthalpy, which is ascribed to the strong interaction between the functional NH_2 group on the pore surface of MOF **6** and CO_2 molecules.[25] Compared with the MOFs reported thus far, the adsorption enthalpy of **6** is higher than those of MOFs such as IRMOF-3 (17.4 kJ mol^{-1}),[26] MOF-177 (15.7 kJ mol^{-1})[27] and PCN-61.[28] However, it is lower than those of bio-MOF-11 (45 kJ mol^{-1})[29] and $Zn_2(Atz)_2(ox)$ (40.8 kJ mol^{-1}).[30] Another point that should be noticed is that the CO_2 adsorption enthalpies of MOFs **1–6** are all higher than that of **1-DABCO**. This may be attributed to the different nature of sp^2 carbon in pyz derivatives and sp^3 carbon in DABCO.[31] The results definitively demonstrate that the sorption properties of MOFs are able to be fine-tuned by introducing definite substituent groups decorated on the pore surface.

To further assess the functionality of the MOFs with specific substituent groups, the catalytic performance of **1** and **6** was studied for the Knoevenagel condensation reactions (Scheme 2).[32] Fig. 3b shows the results of the catalytic condensation of benzaldehyde with ethyl cyanoacetate at 353 K. It was found that **6** accelerated the reaction with a good yield compared with **1** and without using a catalyst. There are free amino groups on the surface of MOF **6**, and the results imply that the reaction occurred within the amino-modified surface of MOF. It is known that mixtures of *E*- and *Z*-isomers were obtained from the conventional Knoevenagel condensation reactions.[33] It should be noted that the *E*-selectivity was observed in our MOF catalyzed reactions and no isomerization of *Z*-form to *E*-form was observed (Fig. S42†), which means that the reaction is controlled thermodynamically. This is rarely observed in previous studies.[34] To extend the application scope, the Knoevenagel condensation of various aldehydes (including electron-donating and electron-withdrawing aromatic aldehydes) with ethyl cyanoacetate has been investigated in the presence of MOF **6**. All the corresponding products can be obtained in good yields and excellent *E*-configuration selectivity (Table S4†). To obtain mechanistic insights into the reactions, the reaction of **6** and PhCHO was performed first. Before the reaction, the solvent DMF of single crystal **6** was completely replaced with cyclohexane. Then the solvent-exchanged samples were immersed in a cyclohexane solution

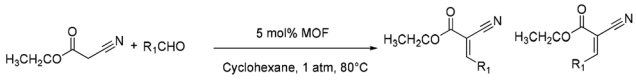

Scheme 2 Knoevenagel condensation of varied benzaldehyde with ethyl cyanoacetate.

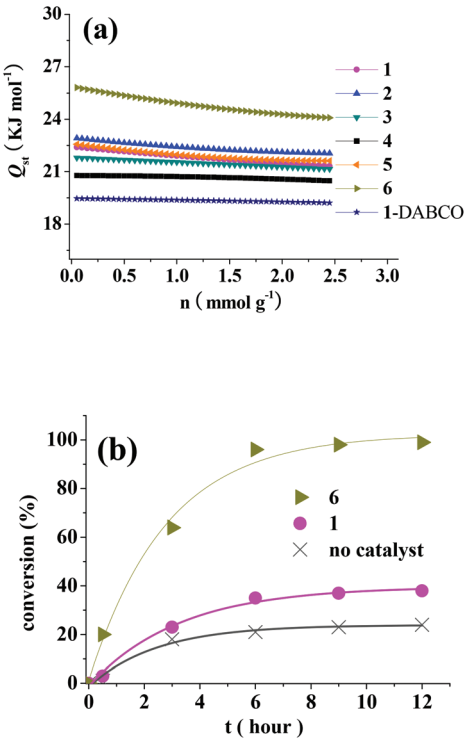

Fig. 3 Gas sorption and catalytic properties. (a) The isosteric adsorption enthalpies for **1–6** and **1-DABCO**. (b) Conversion (%) *vs.* time (hour) for the Knoevenagel condensation reaction of 2 mmol of benzaldehyde with 2 mmol of ethyl cyanoacetate in cyclohexane at 353 K with no catalyst (gray cross), 0.1 mmol of **1** (red circle) and 0.1 mmol of **6** (dark-yellow triangle).

of PhCHO at 85 °C for 24 h. The formation of imine in the pore was observed from the crystal structural analysis (Scheme 3). Although the NH_2 group before the reaction could exist both in small cage A and large cage B, the phenyl ring from PhCHO could only exist in small cage A after the reaction.

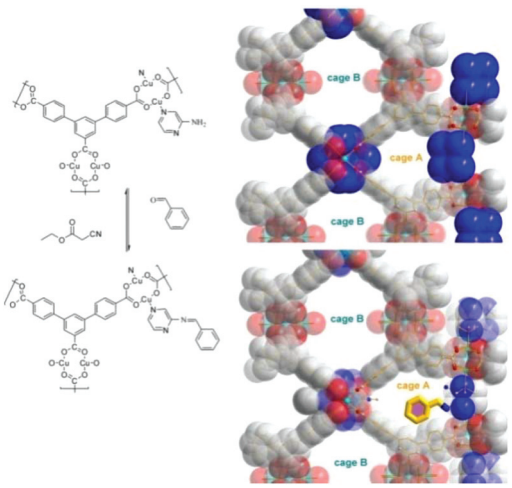

Scheme 3 Schematic representation of the Knoevenagel reaction in the MOFs.

The next reaction of **6**-imine with ethyl cyanoacetate at room temperature was too fast to be observed (less than 5 min) in the crystal structural analysis, resulting in **6** with 2-NH_2-pyz. All these results affirm that the Knoevenagel reactions took place in the small cage in the crystal. Similar reactions with *tert*-butyl 2-cyanoacetate failed due to the large steric repulsion from the *tert*-butyl group and the *Z*-isomers being fewer than the *E*-isomers in the reaction can be probably ascribed to the steric effects. The recyclability of **6** in the Knoevenagel condensation was examined. The catalyst of **6** was easily isolated from the reaction system by centrifugation and could be reused without any loss of activity (Fig. S43†). The PXRD patterns of **6** before and after the reactions were the same, indicating the high stability of **6**.

Conclusions

In conclusion, we have demonstrated the complete and definite ligand exchange of MOF $[Cu_3(L)_2(pyz)(H_2O)]\cdot 13DMF$ (**1**) by pyz derivatives. The merits of such ligand exchange not only provide a way to prepare new MOFs, particularly for the preparation of those not available by direct synthesis, but also enhance and improve the functionality of MOFs through the introduction of functional groups into the pore surface of MOFs. The results of this work show that the internal surface of MOFs can be modified through the introduction of different functional groups *via* easy and fast ligand exchange in the system. A typical example of MOF **6** with 2-NH_2-pyz linkers is given. The introduction of amino group into MOF **6** leads to the largest CO_2 adsorption enthalpy and catalytic reactivity for Knoevenagel condensation reactions. The present study further shows that the ligand exchange is an invaluable synthesis tool and will guide the design and synthesis of new functionalized MOFs.[35]

Acknowledgements

This work was financially supported by the National Natural Science Foundation of China (Grant No. 21331002, 21573106 and 21671097) and the China Postdoctoral Science Foundation (Grant No. 2013M541639). The authors extend their appreciation to the International Scientific Partnership Program ISPP at King Saud University for funding this research work through ISPP#0090. This work was also supported by a Project Funded by the Priority Academic Program Development of Jiangsu Higher Education Institutions.

Notes and references

1 O. K. Farha, A. Özgür Yazaydın, I. Eryazici, C. D. Malliakas, B. G. Hauser, M. G. Kanatzidis, S. T. Nguyen, R. Q. Snurr and J. T. Hupp, *Nat. Chem.*, 2010, **2**, 944–948.
2 A. J. Cairns, J. Eckert, L. Wojtas, M. Thommes, D. Wallacher, P. A. Georgiev, P. M. Forster, Y. Belmabkhout,

J. Ollivier and M. Eddaoudi, *Chem. Mater.*, 2016, **28**, 7353–7361.
3 L. E. Kreno, K. Leong, O. K. Farha, M. Allendorf, R. P. Van Duyne and J. T. Hupp, *Chem. Rev.*, 2011, **112**, 1105–1125.
4 Z.-Z. Lu, R. Zhang, Y.-Z. Li, Z.-J. Guo and H.-G. Zheng, *J. Am. Chem. Soc.*, 2011, **133**, 4172–4174.
5 L. E. Kreno, J. T. Hupp and R. P. Van Duyne, *Anal. Chem.*, 2010, **82**, 8042–8046.
6 F.-J. Song, C. Wang, J. M. Falkowski, L.-Q. Ma and W.-B. Lin, *J. Am. Chem. Soc.*, 2010, **132**, 15390–15398.
7 X.-L. Lv, K. Wang, B. Wang, J. Su, X. Zou, Y. Xie, J.-R. Li and H.-C. Zhou, *J. Am. Chem. Soc.*, 2017, **139**, 211–217.
8 N. Stock and S. Biswas, *Chem. Rev.*, 2011, **112**, 933–969.
9 S. Ma, D. Sun, J. M. Simmons, C. D. Collier, D. Yuan and H.-C. Zhou, *J. Am. Chem. Soc.*, 2007, **130**, 1012–1016.
10 P. Wang, L. Luo, J. Fan, G.-C. Lv, Y. Song and W.-Y. Sun, *Microporous Mesoporous Mater.*, 2013, **175**, 116–124.
11 S.-S. Chen, M. Chen, S. Takamizawa, P. Wang, G.-C. Lv and W.-Y. Sun, *Chem. Commun.*, 2011, **47**, 4902–4904.
12 Z. Wang and S. M. Cohen, *Chem. Soc. Rev.*, 2009, **38**, 1315–1329.
13 D. J. Xiao, J. Oktawiec, P. J. Milner and J. R. Long, *J. Am. Chem. Soc.*, 2016, **138**, 14371–14379.
14 J. a. Zhao, L. Mi, J. Hu, H. Hou and Y. Fan, *J. Am. Chem. Soc.*, 2008, **130**, 15222–15223.
15 P. Deria, J. E. Mondloch, O. Karagiaridi, W. Bury, J. T. Hupp and O. K. Farha, *Chem. Soc. Rev.*, 2014, **43**, 5896–5912.
16 M. Kim, J. F. Cahill, Y. Su, K. A. Prather and S. M. Cohen, *Chem. Sci.*, 2012, **3**, 126–130.
17 D. Yang, V. Bernales, T. Islamoglu, O. K. Farha, J. T. Hupp, C. J. Cramer, L. Gagliardi and B. C. Gates, *J. Am. Chem. Soc.*, 2016, **138**, 15189–15196.
18 K. Biradha, Y. Hongo and M. Fujita, *Angew. Chem., Int. Ed.*, 2002, **41**, 3395–3398.
19 C. Hou, Q. Liu, J. Fan, Y. Zhao, P. Wang and W.-Y. Sun, *Inorg. Chem.*, 2012, **51**, 8402–8408.
20 T. Haneda, M. Kawano, T. Kawamichi and M. Fujita, *J. Am. Chem. Soc.*, 2008, **130**, 1578–1579.
21 T. Li, M. T. Kozlowski, E. A. Doud, M. N. Blakely and N. L. Rosi, *J. Am. Chem. Soc.*, 2013, **135**, 11688–11691.
22 H. Deng, C. J. Doonan, H. Furukawa, R. B. Ferreira, J. Towne, C. B. Knobler, B. Wang and O. M. Yaghi, *Science*, 2010, **327**, 846–850.
23 J. K. Schnobrich, O. Lebel, K. A. Cychosz, A. Dailly, A. G. Wong-Foy and A. J. Matzger, *J. Am. Chem. Soc.*, 2010, **132**, 13941–13948.
24 T. Düren, L. Sarkisov, O. M. Yaghi and R. Q. Snurr, *Langmuir*, 2004, **20**, 2683–2689.
25 J. Park, Z. U. Wang, L.-B. Sun, Y.-P. Chen and H.-C. Zhou, *J. Am. Chem. Soc.*, 2012, **134**, 20110–20116.
26 A. R. Millward and O. M. Yaghi, *J. Am. Chem. Soc.*, 2005, **127**, 17998–17999.
27 A. Ö. Yazaydın, R. Q. Snurr, T.-H. Park, K. Koh, J. Liu, M. D. LeVan, A. I. Benin, P. Jakubczak, M. Lanuza, D. B. Galloway, J. J. Low and R. R. Willis, *J. Am. Chem. Soc.*, 2009, **131**, 18198–18199.
28 D. Yuan, D. Zhao, D. Sun and H.-C. Zhou, *Angew. Chem., Int. Ed.*, 2010, **49**, 5357–5361.
29 J. An, S. J. Geib and N. L. Rosi, *J. Am. Chem. Soc.*, 2009, **132**, 38–39.
30 R. Vaidhyanathan, S. S. Iremonger, G. K. H. Shimizu, P. G. Boyd, S. Alavi and T. K. Woo, *Science*, 2010, **330**, 650–653.
31 E. D. Bloch, W. L. Queen, R. Krishna, J. M. Zadrozny, C. M. Brown and J. R. Long, *Science*, 2012, **335**, 1606–1610.
32 T. Gadzikwa, O. K. Farha, C. D. Malliakas, M. G. Kanatzidis, J. T. Hupp and S. T. Nguyen, *J. Am. Chem. Soc.*, 2009, **131**, 13613–13615.
33 S. Zhao, Y. Chen and Y.-F. Song, *Appl. Catal., A*, 2014, **475**, 140–146.
34 R. Tanikaga, N. Konya, K. Hamamura and A. Kaji, *Bull. Chem. Soc. Jpn.*, 1988, **61**, 3211–3216.
35 O. Karagiaridi, W. Bury, J. E. Mondloch, J. T. Hupp and O. K. Farha, *Angew. Chem., Int. Ed.*, 2014, **53**, 4530–4540.